Supporting Information

Triboelectric Nanogenerator Ion Mobility-Mass Spectrometry for In-Depth Lipid Annotation.

Marcos Bouza[‡, †], Yafeng Li[‡], Aurelia C. Wang[§], Zhong L. Wang[§, ‖], Facundo M. Fernández[‡, †].

[‡]School of Chemistry and Biochemistry, Georgia Institute of Technology, Atlanta, GA 30332, USA.

[†]NSF/NASA Center for Chemical Evolution, Atlanta, GA 30332, USA.

[§]School of Materials Science and Engineering, Georgia Institute of Technology, Atlanta, GA 30332, USA.

[‖]Beijing Institute of Nanoenergy and Nanosystems, Chinese Academy of Sciences, National Center for Nanoscience and Technology (NCNST), Beijing 100083, China.

[*]Corresponding author: facundo.fernandez@chemistry.gatech.edu

Table of Contents

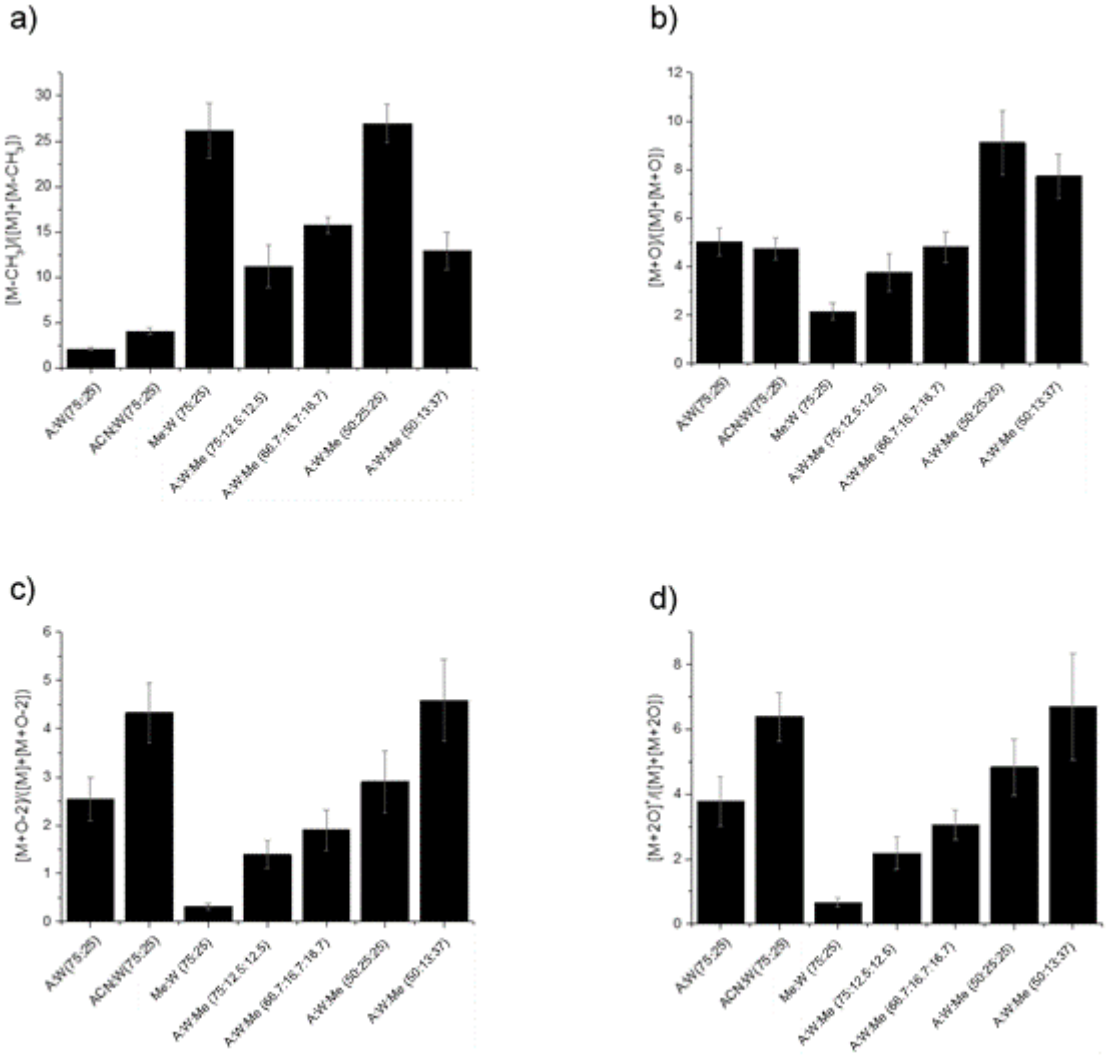

Figure S1. Optimization of the solvent system used for unsaturated lipid TENG IM-MS analysis. LysoPC(18:1(9Z)) at a 20 µM concentration with 25 mM of NH_4OAc was analyzed in negative ion mode. Abundance ratios of ionic species at *m/z* 566.4 $[M\text{-}CH_3+OAc]^-$, *m/z* 580.4 $[M+OAc]^-$, *m/z* 594.4 $[MO\text{-}2H+OAc]^-$, *m/z* 596.4 $[MO+OAc]^-$, and *m/z* 612.4 $[M+2O+OAc]^-$ were compared. a) 566.4/(580.4+566.4) demethylation ratio, b) 596.4/(580.4+596.4) double bond epoxidation ratio, c) *m/z* 594.4/(580.4+594.4) ratio indicating epoxidation of a saturated bond and d) *m/z* 612.4/(580.4+612.4) peroxidation ratio.

In order to find an appropriate solvent system for TENG TAP IM-MS analysis, different solvents, including acetone (A), acetonitrile (ACN) or methanol (Me) were tested. A necessary condition for this type of experiment is the presence of small amounts of water (W) to boost the conductivity of the solution so as to favor the formation of the glow corona discharge at the emitter tip. Without this discharge, which is formed concomitantly with the pulsed spray, no detectable lipid epoxidation is observed (see Figure S2). The optimum solvent system was selected by favoring a simpler mass spectrum while maintaining the highest epoxidation yields possible. Corona discharge effects were more appreciable in negative ion mode, as expected. For this reason, adduction of glycerophospholipids with acetate anions using 25 mM NH_4OAc as the additive was used to favor higher sensitivity experiments. The results shown above present the ratios for the methyl group loss at *m/z* 566.4 ($[M\text{-}CH_3+OAc]^-$), the singly epoxidized species at *m/z* 596.4 ($[MO+OAc]^-$), the epoxidation of saturated bonds leading to the ion at *m/z* 594.4 ($[MO\text{-}2H+OAc]^-$), and the peroxidation product ion at *m/z* 612.4 ($[M+2O+OAc]^-$) against the abundance of the acetate adduct ion at *m/z* 580.4 ($[M+OAc]^-$). All solvent systems examined promoted double bond epoxidation, but with large yield differences (Figure S1b). The presence of acetone was also decisive for boosting

the epoxidation yield. Even though a combination of A:W:Me (50:25:25) showed the highest relative $[MO+OAc]^-$ yields, the formation of side products that decreased the absolute abundance of $[M+OAc]^-$, and therefore $[MO+OAc]^-$, made this choice less desirable. It was also observed that the proportion of M had a deep effect on the fragmentation extent of the choline group during the ionization process, promoting the formation of the *m/z* 566.4 species (Figure S1a). In the same manner, we also observed that higher ratios of organic solvents promoted non-specific oxidation to species such as $[MO-2H+OAc]^-$ and $[M+2O+OAc]^-$. Based on such observations, the solvent system chosen as a compromise was A:W:Me (75:12.5:12.5).

In the experiments shown here, acetone seems to play a different role than in Paternò-Büchi reactions used for lipid double bond pinpointing. In general, the enhanced solubility of lipids in acetone likely makes larger amounts of lipids available for oxidation, therefore boosting the associated signals. However, in the case of TENG experiments, oxidation has been shown to occur in the gas-phase and not in condensed phase.[1] A small amount of water is mandatory for sustaining the TENG corona discharge, but the different co-solvents seem to have a significant effect in the lipid oxidation process. The most likely reaction mechanism for TENG gas-phase lipid oxidation proceeds *via* hydroxyl, oxygen and/or superoxygen radicals. Although all the evaluated co-solvents led to lipid oxidation, they showed markedly different efficiencies in producing the desired reaction products. Methanol:water mixtures, for example, yielded the lowest oxidation efficiencies. Methanol is known as a hydroxyl radical scavenger in DC corona discharges,[2] with its presence leading to a reduction in the population of gas-phase radical species. Our experiments also show that when acetone is present in solution, the oxidation efficiency is boosted. Acetone has been reported to favor intermediate radical species that lead to greater abundances of hydroxyl or oxygen radicals, [3] in agreement with the above observations. Further experiments should be conducted to better establish the role of acetone in gas-phase TENG-induced oxidation reactions, in an effort to improve our understanding of the underlying ionization/oxidation mechanisms.

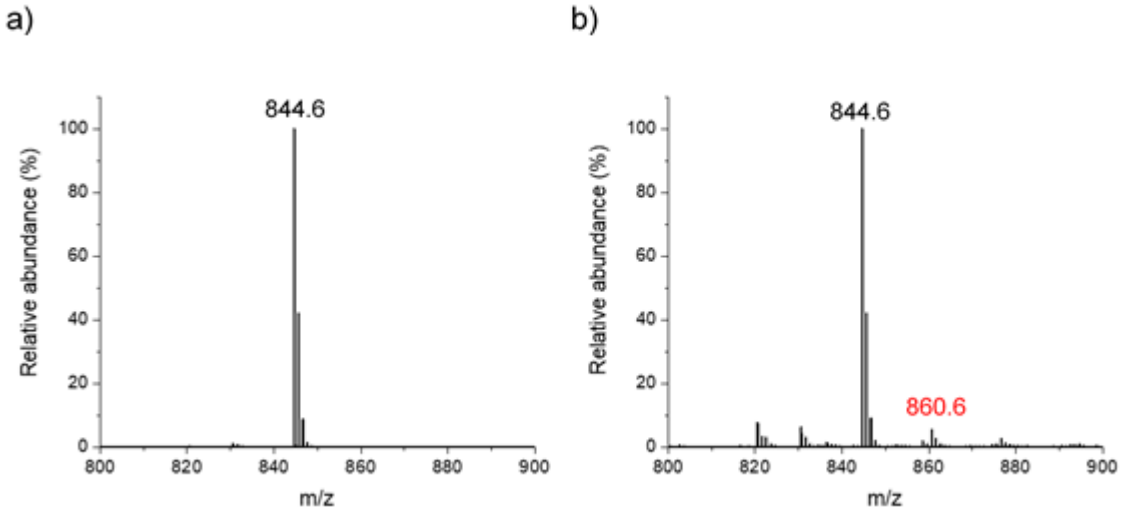

Figure S2. Negative ion mode MS analysis of a 20 µM PC(18:1(9*Z*)/18:1(9*Z*)) in acetone:water:methanol (75:12.5:12.5) with 25 mM NH_4OAc added. a) NanoESI and b) TENG.

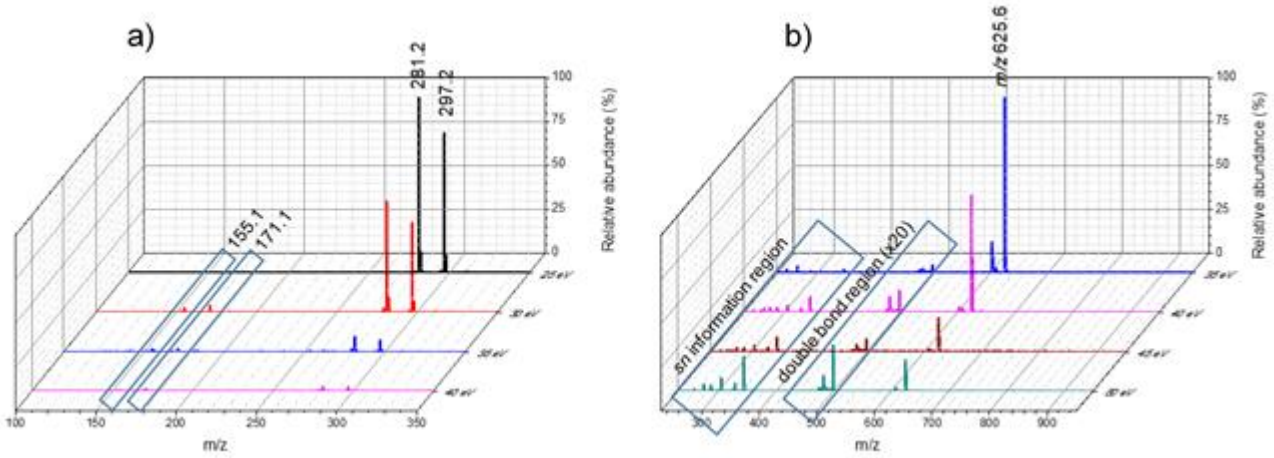

Figure S3. Evaluation of the fragmentation efficiency for TENG TAP MS/MS using a 20 µM solution of PC(18:1(9Z)/18:1(9Z)) in acetone:water:methanol (75:12.5:12.5). Mass spectra for a) negative ion mode analysis using 25 mM NH_4OAc as an additive, and a 50 eV trap collision cell energy, and b) positive ion mode using 5 mM LiOAc as the additive and 35 eV trap collision cell energy. Univariate optimization was performed: first, the trap cell collision energy was optimized followed by the transfer cell collision energy.

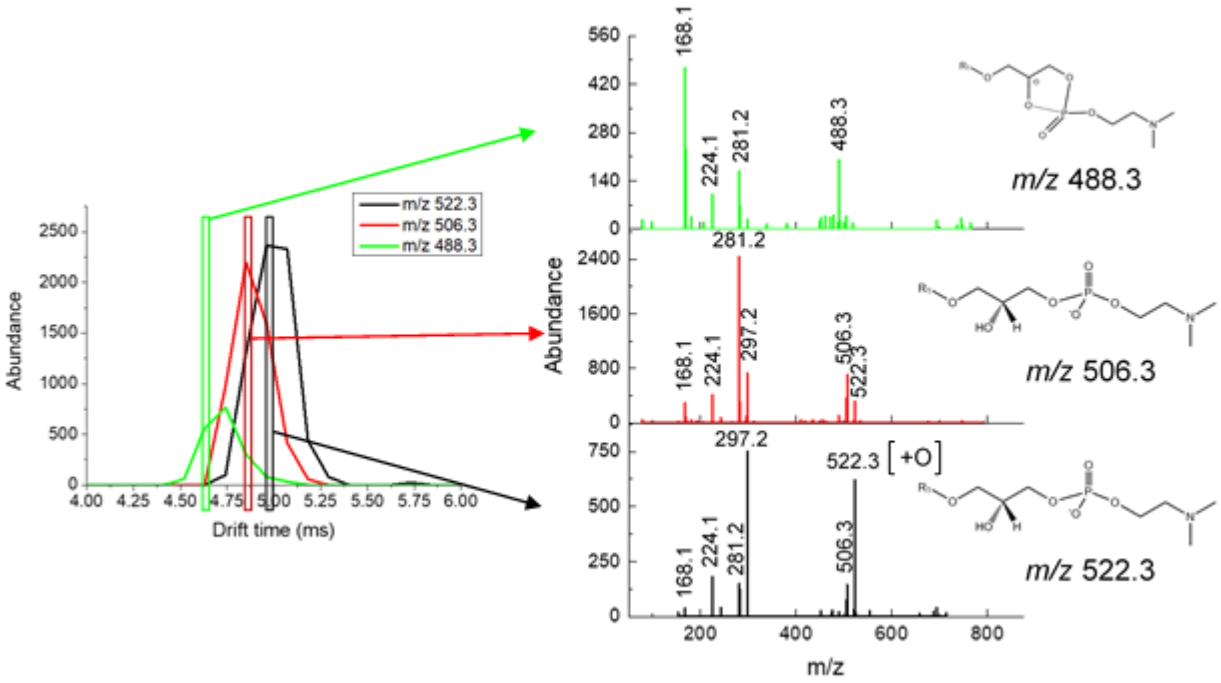

Figure S4. Negative ion mode arrival time distributions (ATD) and corresponding TENG TAP mass spectra for three different PC(18:1(*9Z*)/18:1(*9Z*)) ion species in the 4.25-5.50 ms IM range. Figure 2e in the main text results from averaging across this entire mobility range. The detected fragment ions only informed about acyl chain composition, but not *sn*-chain position. This is caused by the equivalency of the observed fragmentation pathways for both regioisomers. The most notable fragment ions were:

- *m/z* 488.3: primary fragment resulting from the neutral loss of RCOOH from the sn_1 or sn_2 position (R=$C_{17}H_{33}O$), loss of CH_3, and acetate from *m/z* 860.6. In the ion structure, R_1=$C_{18}H_{33}O$.
- *m/z* 506.3: primary fragment resulting from the neutral loss of a ketene (RCH=C=O) from the sn_1 or sn_2 position (R=$C_{16}H_{29}O$), CH_3 and acetate from *m/z* 860.6. In the ion structures, R_1=$C_{18}H_{33}O$. A fragment ion of an equivalent mass is obtained for the epoxidated *m/z* 488.3 fragment ion with R_1=$C_{18}H_{33}O_2$.
- *m/z* 522.3: analog of the *m/z* 506.3 primary fragment ion with an epoxidized R_1= $C_{18}H_{33}O_2$ acyl chain.

In the lower *m/z* range several fragment ions should also be highlighted:

- *m/z* 297.2: epoxidized $[C_{18}H_{33}O_3]^-$ 18:1 fatty acyl chain from either the sn_1 or sn_2 position.
- *m/z* 281.2: $[C_{18}H_{33}O_2]^-$ 18:1 fatty acyl chain from either the sn_1 or sn_2 position.
- *m/z* 224.1: glycerophosphocholine fragment followed by loss of CH_3 and H_2O.
- *m/z* 168.1: phosphocholine fragment followed by loss of CH_3.

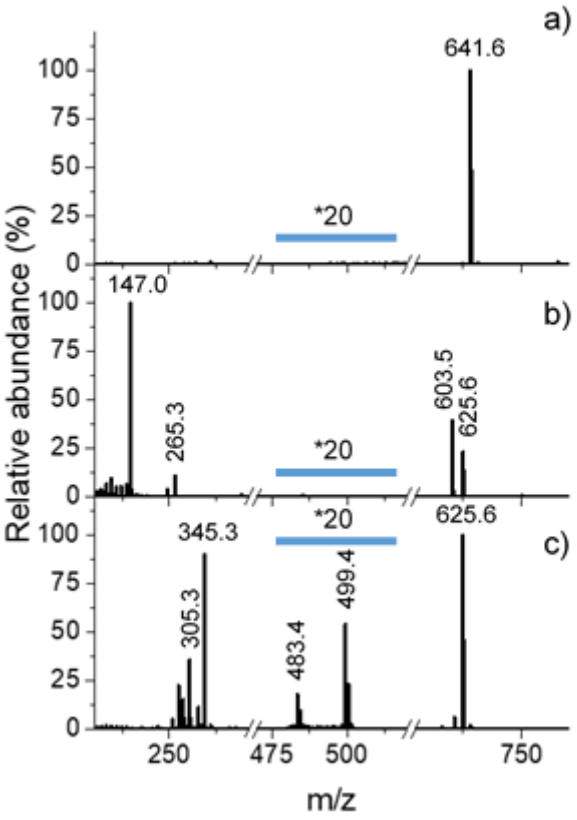

Figure S5. Positive ion mode TENG TAP IM-MS spectra for a 20 µM PC(18:1(9*Z*)/18:1(9*Z*)) solution in acetone:water:methanol (75:12.5:12.5). a) Fragmentation spectrum obtained for the $[MO+Na]^+$ precursor ion at *m/z* 824.6, b) Fragmentation spectrum for the $[M+Na]^+$ precursor ion at *m/z* 808.6 and c) Fragmentation spectrum for the $[MO+Li]^+$precursor ion at *m/z* 808.6.

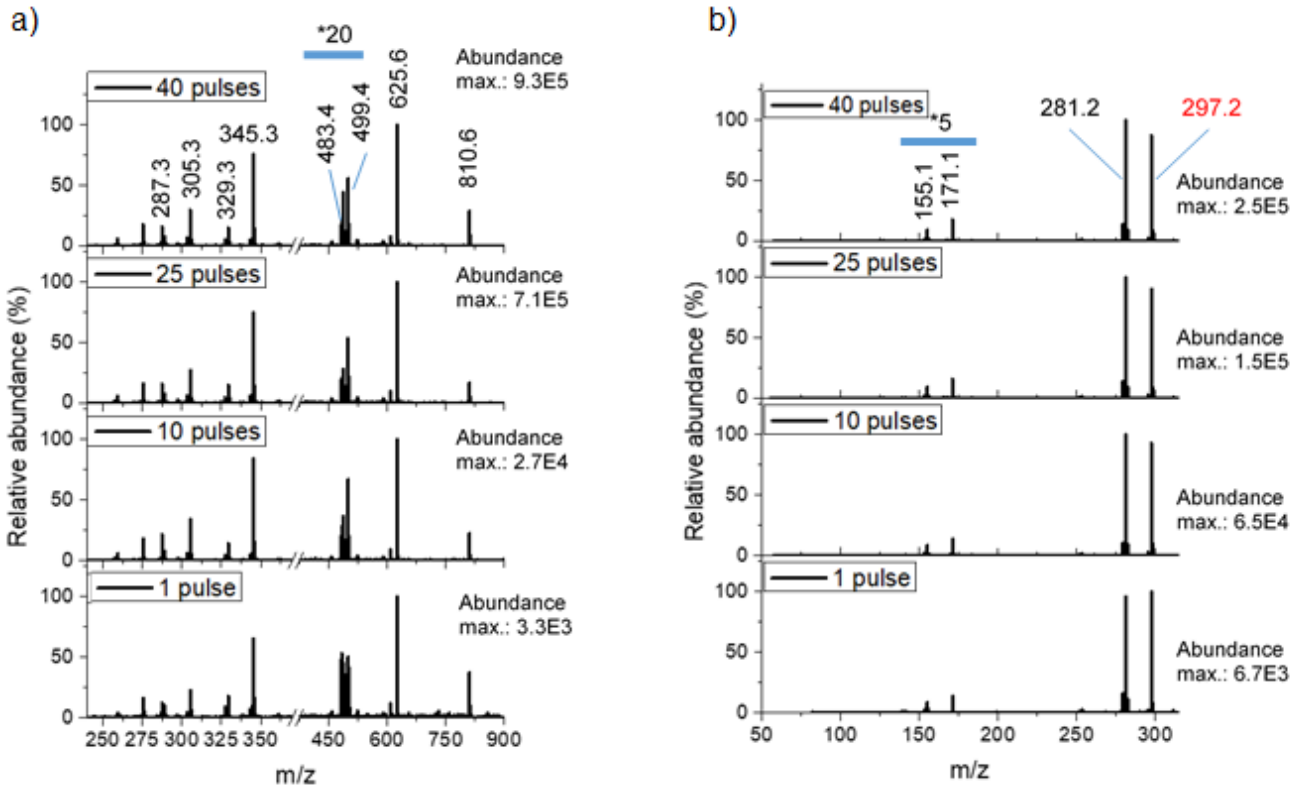

Figure S6. Effect of the number of TENG pulses on the abundance of the various fragment ions observed for 20 µM PC(18:1(9*Z*)/18:1(9*Z*)) using 25 mM NH_4OAc as an additive in negative ion mode, and 5 mM LiOAc in positive ion mode. Spectra shown for the regions corresponding to a) *sn*-position and double bond position diagnostic fragments at *m/z* 345.3, 361.3, 329.3, 303.3 and 287.3, and 499.4, 483.4, in positive ion mode. One, ten, twenty and forty TENG spray pulses were collected, and b) double bond position diagnostic fragments at *m/z* 155.1 and 171.1 in negative ion mode.

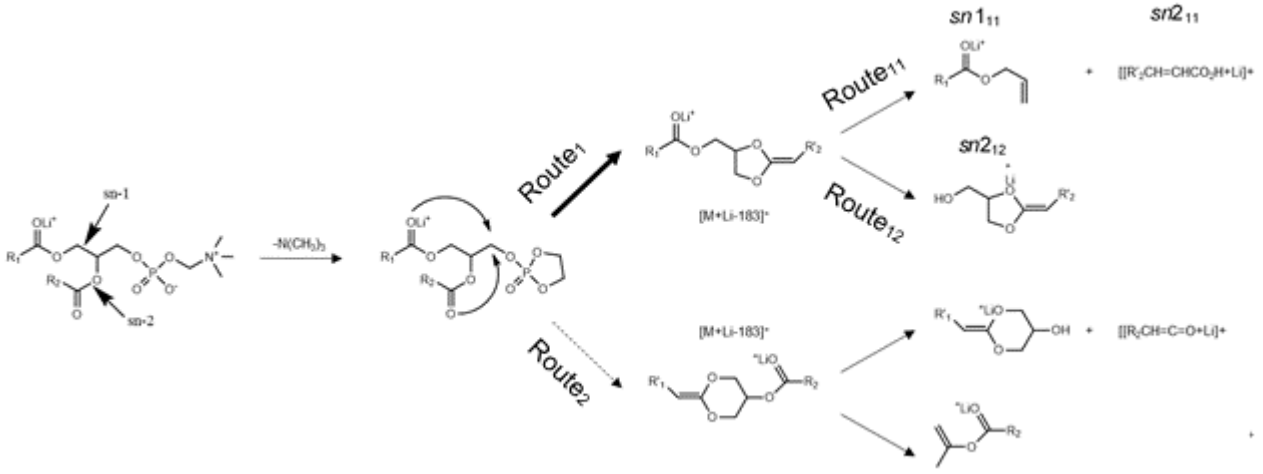

Figure S7. Fragmentation pathway for lithium-adducted phosphocholines, enabling *sn*-position elucidation.[4]

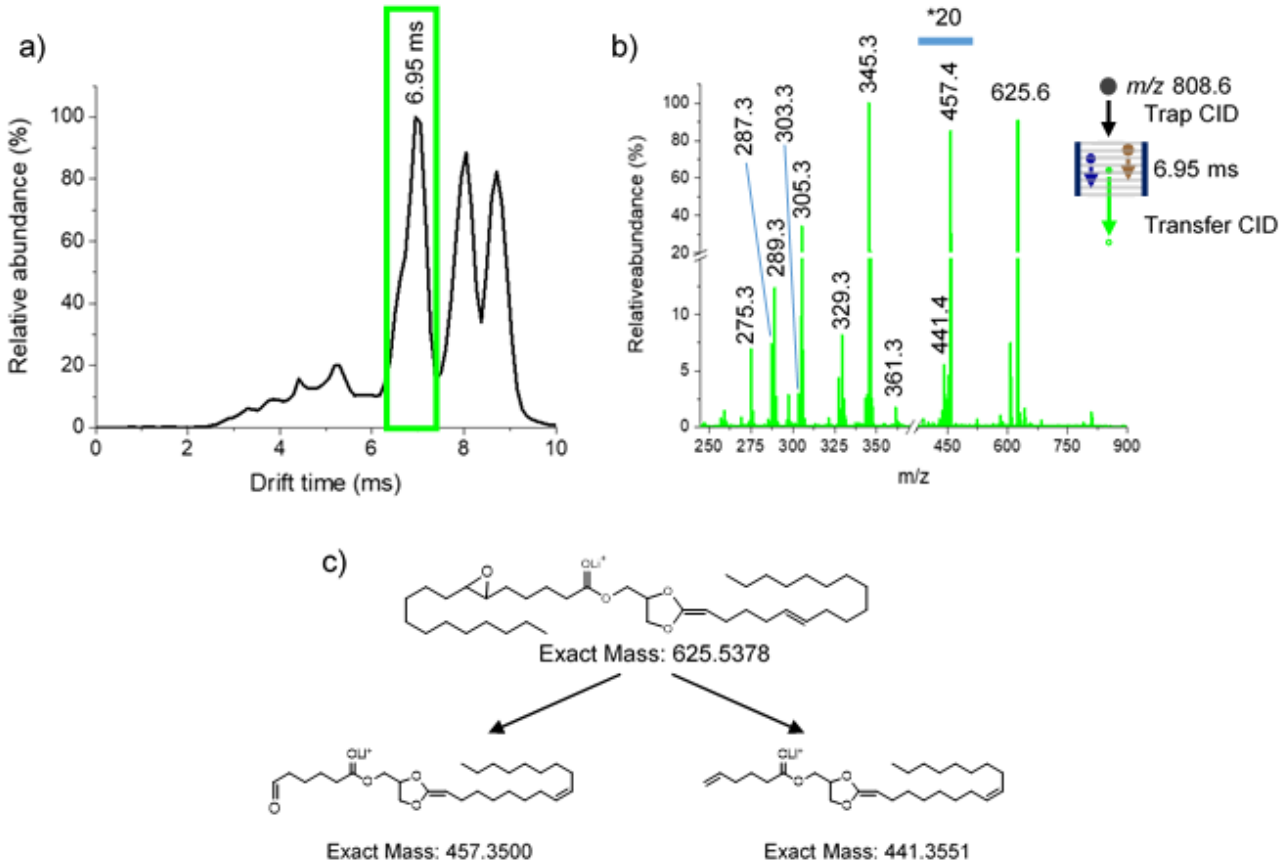

Figure S8. Positive ion mode analysis of 20 µM PC(18:1(*6Z*)/18:1(*6Z*)) in acetone:water:methanol (75:12.5:12.5) with 5 mM LiOAc. a) Total ion ATD following selection and trap CID of the $[MO+Li]^+$ ion (*m/z* 808.6). The green box represents the region corresponding to the dioxolane fragment ion at *m/z* 625.6, b) TAP transfer CID spectrum of the group of fragment ions outlined with the green box in a) . c) Proposed structures for diagnostic fragments species at *m/z* 457.4 and 441.4, indicating Δ6 double bond position.

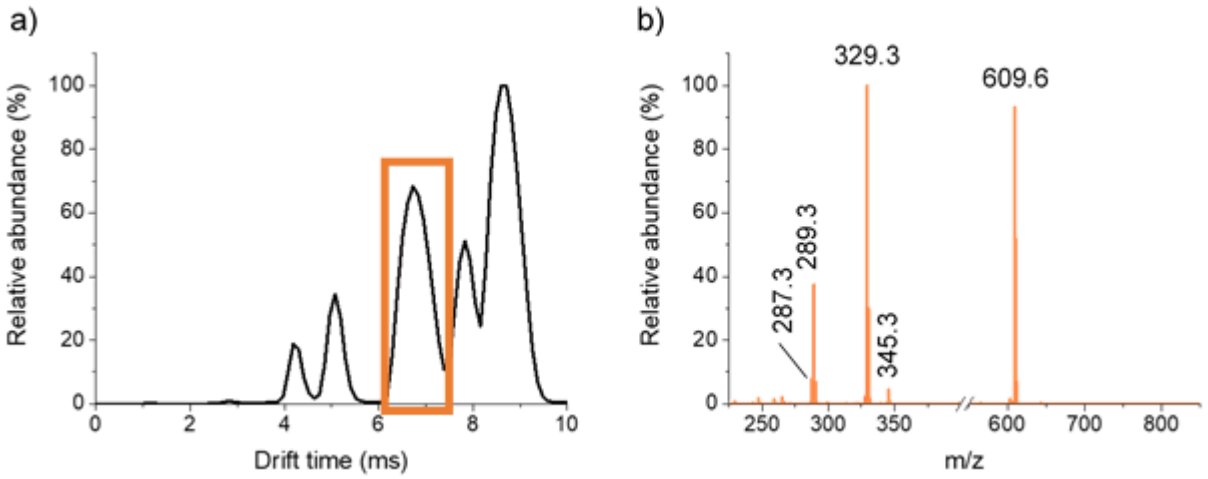

Figure S9. Positive ion mode TENG TAP IM-MS of 20 µM PC(18:1(*9Z*)/18:1(*9Z*)) in acetone:water:methanol (75:12.5:12.5) with 5 mM LiOAc added. The $[M+Li]^+$ precursor ion at *m/z* 792.6 was quadrupole selected. a) Total ion ATD, with the dioxolane ion region highlighted with the orange box (maximum at 6.6 ms). b) TAP transfer CID spectrum of the group of fragment ions outlined in a). The ion at *m/z* 609.6 corresponded to the 5 five member dioxolane species, that further fragmented into *m/z* 287.3, 329.3 and 345.3, yielding *sn*-position information.

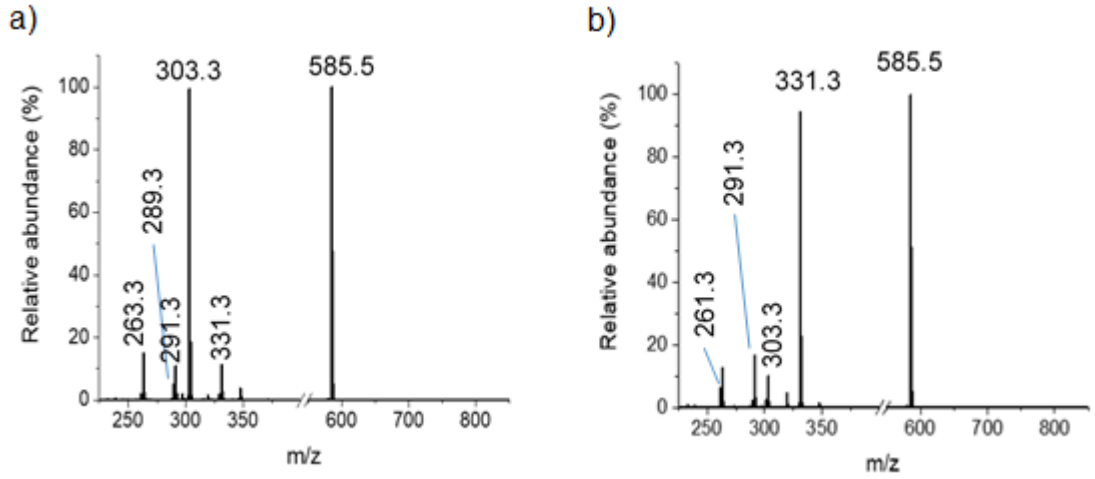

Figure S10. Positive ion mode TENG TAP IM-MS results for the arrival time region corresponding to the dioxolane fragment ion of**:** a) PC (16:0/18:0) and b) PC (18:0/16:0).

TAP transfer CID spectra of the dioxolane ATD region for PC (16:0/18:0) and PC (18:0/16:0) regioisomers yielded different product ions, enabling to determine their fatty acyl (FA) chain stereospecificity. The fragments produced by Route$_{11}$ (Figure S6) were different for each one of the regioisomers: *m/z* 303.3 (fragment *sn1*$_{11}$ for the 16:0 fatty acyl chain) and 289.3 (fragment *sn2*$_{11}$ for the 18:0 fatty acyl chain) for PC (16:0/18:0), and *m/z* 331.3 (fragment *sn1*$_{11}$ for the 18:0 fatty acyl chain) and 261.3 (fragment *sn2*$_{11}$ for the 16:0 fatty acyl chain) for PC (18:0/16:0). Fragments corresponding to Route$_{12}$ were detected with lower abundances: *m/z* 273.3 (*sn2*$_{12}$) for PC (18:0/16:0) and *m/z* 245.2 (*sn2*$_{12}$) for PC (16:0/18:0). Small isomeric impurities were detected by the minor signals at *m/z* 331.3, corresponding to a PC(18:0/16:0) isomer impurity in the PC(16:0/18:0) standard (Figure S9a), and *m/z* 303.3 in Figure S9b. The presence of these impurities has been confirmed by other studies.[5,6]

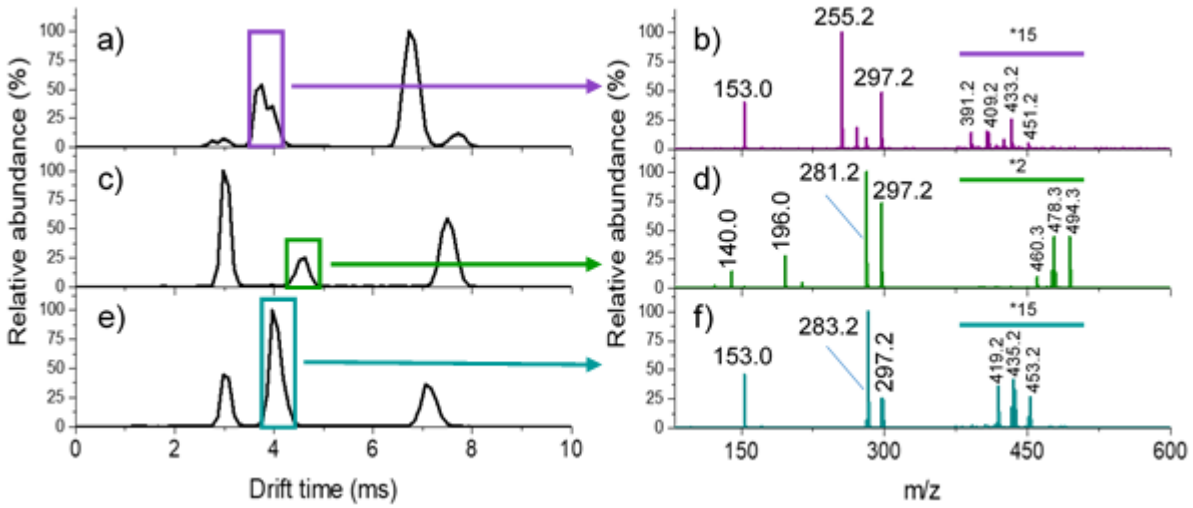

Figure S11. Total ion IM ATD following selection in the quadrupole analyzer and TAP fragmentation of a) PS(16:0/18:1(*9Z*)) $[MO]^-$ at *m/z* 776.6, c) PE(18:1(*9E*)/18:1(*9E*)) $[MO]^-$ at *m/z* 758.6 and e) PA(18:0/18:1(*9Z*)) $[MO]^-$ at *m/z* 717.6. The purple, green and cyan boxes depict the ATD regions producing *sn*-composition information, their TAP product ion spectra are shown in b, d and f. The identities of the product ions observed in negative ion mode were corroborated using the GP product ion calculation tool in LIPID MAPS (https://www.lipidmaps.org/tools/structuredrawing/GP_p_form.php).

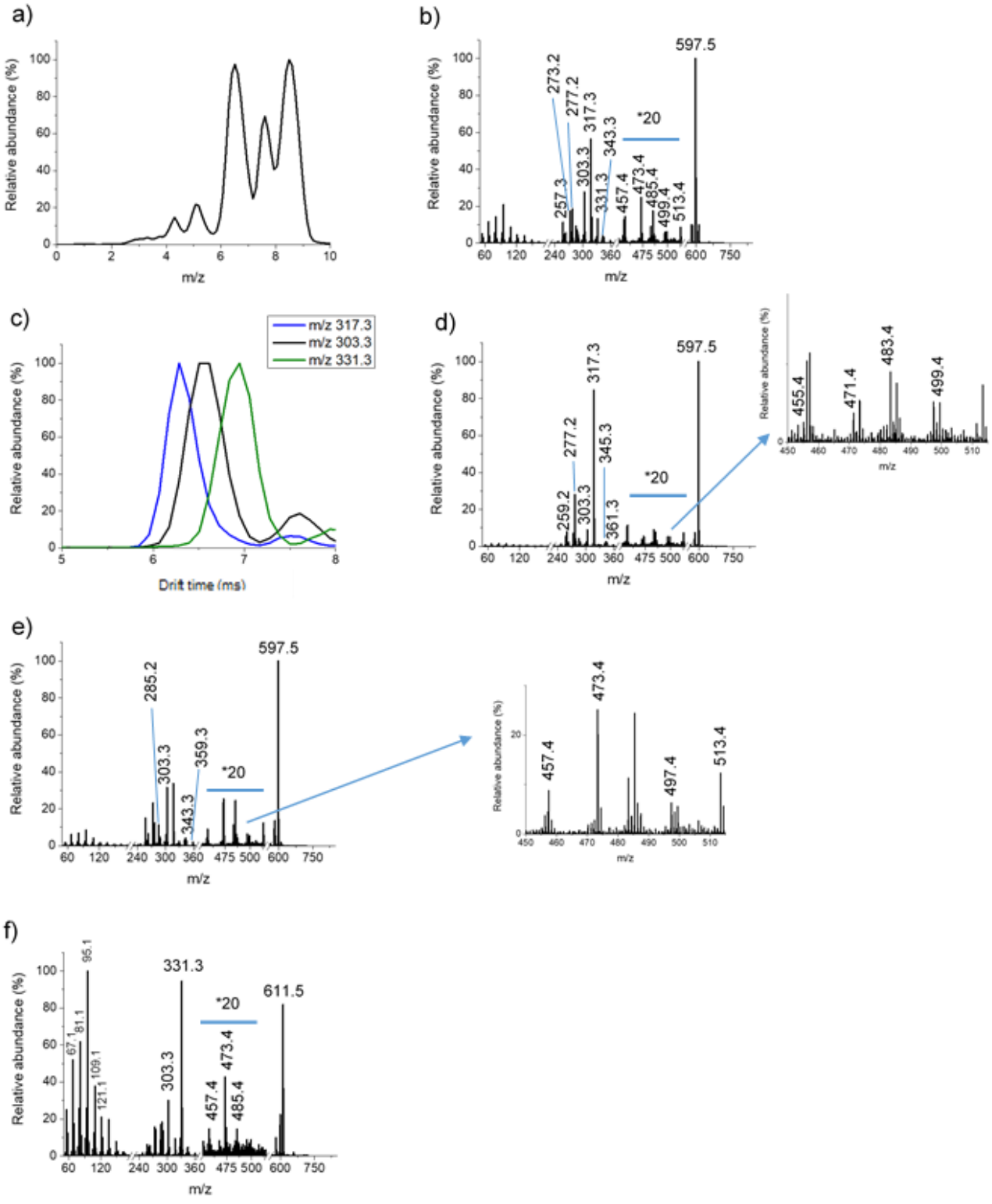

Figure S12. Positive ion mode analysis for multiple isomers of the $[MO+Li]^+$ ion at *m/z* 780.6 in an egg PC extract. a) Total ion ATD for PC(34:2) $[MO+Li]^+$, b) $[MO+Li]^+$ averaged mass spectrum corresponding to the dioxolane ATD region at 6.50 ms, c) mass-selected ATD for diagnostic fragment ions that enable chain *sn*-position assignment. Blue trace: $sn1_{11}$ fragment of PC(16:1/18:1) (Table S1b), black trace: $sn1_{11}$ fragment of PC(16:0_18:2) (Table S1b), and green trace: fragment ion of the [PC(36:1)-14 Da] interference, d) Mass spectrum obtained at the 6.1 ms maximum of the *m/z* 317.3 ATD shown in c). The zoom-in shows a detail of the double bond diagnostic fragment ion region, with assignments detailed in Table S1b, e) Mass spectrum obtained at the 6.6 ms maximum of the *m/z* 303.3 ATD shown in c). The inset shows the double bond diagnostic region (Table S1b), and f) Mass

spectrum obtained at the 7.0 ms maximum of the *m/z* 331.3 ATD shown in c). This mass spectrum corresponds to the isobaric [PC(36:1)-14 Da] interference. The atypical dioxolane product ion at *m/z* 611.5 originates from PC(36:1) with an 18:0 fatty acyl chain in the *sn1* position, as indicated by the fragment ion at *m/z* 331.3.

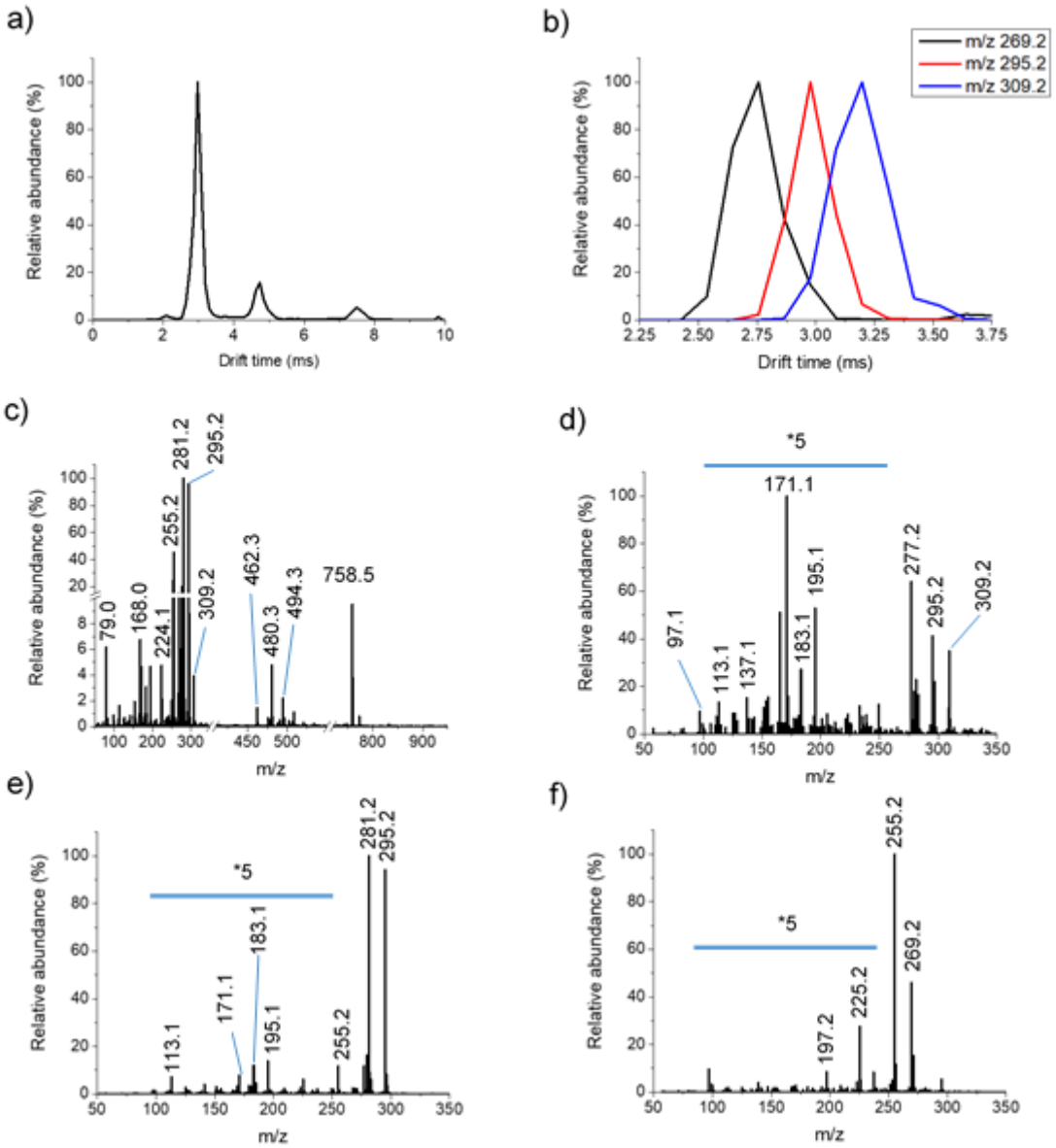

Figure S13. Negative ion mode TENG TAP IM-MS analysis of multiple $[MO+OAc]^-$ PC(34:2) isomers in an egg PC extract. a) Total ion ATD, b) ATD for different $[FA+O-H]^-$ chain fragment ions, c) Average fragmentation spectrum for the ATD peak between 2.30-3.7 ms, d) Fragmentation spectrum for an arrival time of 2.98 ms [red trace in b)], leading to the identification of one PC(34:2) isomer as PC(16:0_18:2(*9*, *12*)) by the fragments listed in Table S2b, e) Fragmentation spectrum corresponding to an arrival time of 2.7 ms [black trace in b)], leading to the identification of a second PC(34:2) isomer as PC(16:1(*9*)_18:1(*9*)) (Table S2b). f) Fragmentation spectrum for an arrival time of 3.2 ms [blue trace in b)], corresponding to the a 20:1 fatty acyl chain fragment ion, likely from PC(14:1_20:1).

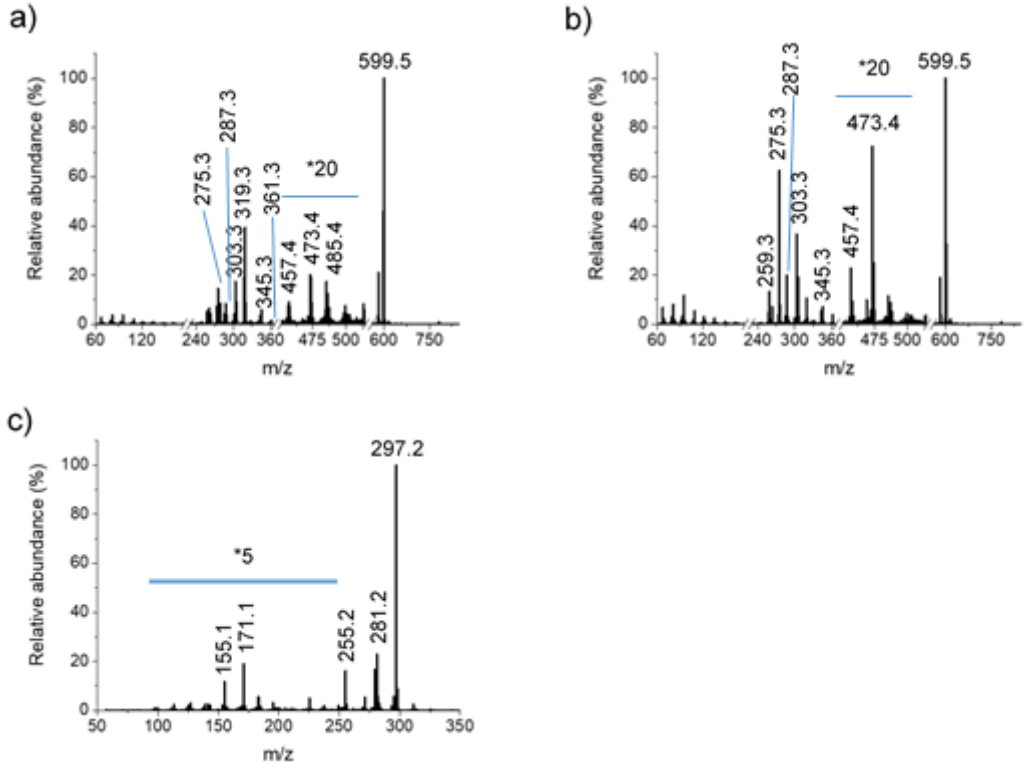

Figure S14. TENG TAP IM-MS analysis of multiple PC (34:1) isomers in an egg PC extract. The $[MO+Li]^+$ ion at *m/z* 782.6 was selected as the precursor for positive ion mode analysis (see fragment annotations in Table S1b). a) Positive ion mode TAP product ion spectrum of the dioxolane ATD region at 6.61 ms corresponding to PC(18:1(9)/16:0). b) Positive ion mode TAP product ion spectrum of the 6.73 ms ATD region corresponding to PC(16:0/18:1(9)). c) Negative ion mode TAP product ion spectrum of the 3.09 ms ATD region corresponding to the $[FA+O-H]^-$ epoxidized 18:1 fatty acyl chain at *m/z* 297.3 (See Table S2b). The PC(16:0_18:1(9)) $[MO+OAc]^-$ ion at *m/z* 834.6 was selected as the precursor ion.

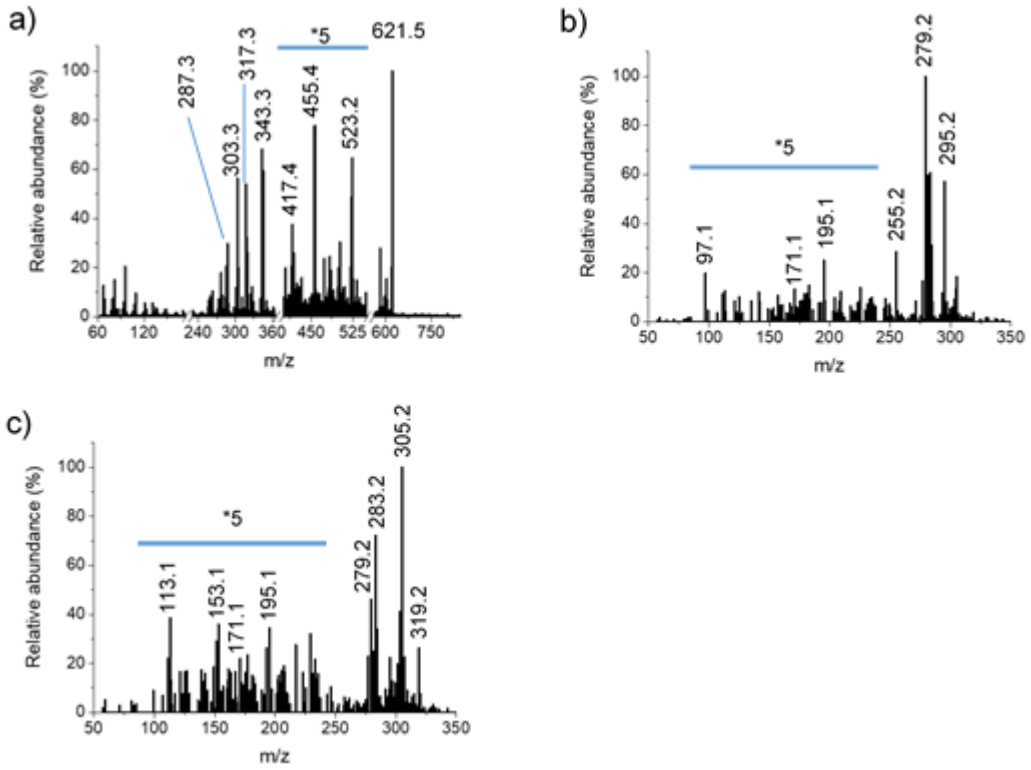

Figure S15. TENG TAP IM-MS analysis of multiple PC (36:4) isomers in an egg PC extract. The $[MO+Li]^+$ ion at *m/z* 804.6 was selected as the precursor ion in positive ion mode, which included the PC(16:0/20:4 (5, 8, 11, 14)), PC(20:4 (5, 8, 11, 14)/16:0), and PC(18:2(9, 12)/18:2(9, 12)) isobars. Fragment annotations are given in Table S1b. For negative ion mode experiments, the $[MO+OAc]^-$ ion at *m/z* 856.6 was selected as the precursor ion. a) Positive ion mode TAP product ion spectrum of the dioxolane ATD region at 6.61 ms. b) Negative ion mode TAP product ion spectrum for the 18:2 $[FA+O-H]^-$ ion (*m/z* 295.2) with an ATD maximum at 2.98 ms. The PC(18:2(9, 12)_18:2(9, 12)) $[MO+OAc]^-$ ion was selected as the precursor ion. c) Negative ion mode TAP product ion spectrum for the 20:4 $[FA+O-H]^-$ ion (*m/z* 319.2) with an ATD maximum at 3.20 ms. The PC(16:0_20:4(5, 8, 11, 14)) $[MO+OAc]^-$ ion was selected as the precursor ion.

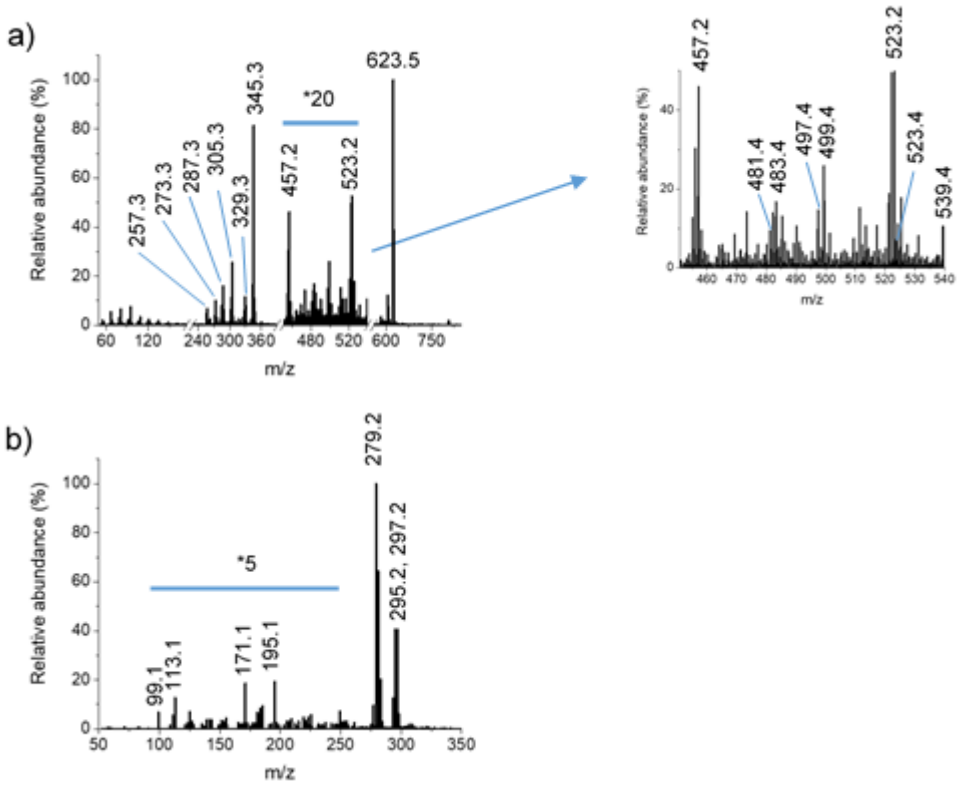

Figure S16. TENG TAP IM-MS analysis of multiple PC (36:3) isomers in an egg PC extract. a) Positive ion mode TAP product ion spectrum of the dioxolane ATD region at 6.84 ms. The $[MO+Li]^+$ ion at *m/z* 806.6 was selected as the precursor ion, which included the PC(16:0/20:3(5, 8, 11)), PC(20:3(5, 8, 11)/16:0), PC(18:1(9)/18:2(9, 12)), PC(18:2(9, 12)/18:1(9)) isobars. Fragment annotations are given in Table S1b. b) Negative ion mode TAP product ion spectrum for the ATD maximum at 2.98 ms, which included both the 18:1 and 18:2 $[FA+O-H]^-$ ions (*m/z* 297.2 and 295.2). The PC(18:1(9)_18:2(9, 12)) $[MO+OAc]^-$ ion at *m/z* 856.6 was selected as the precursor ion.

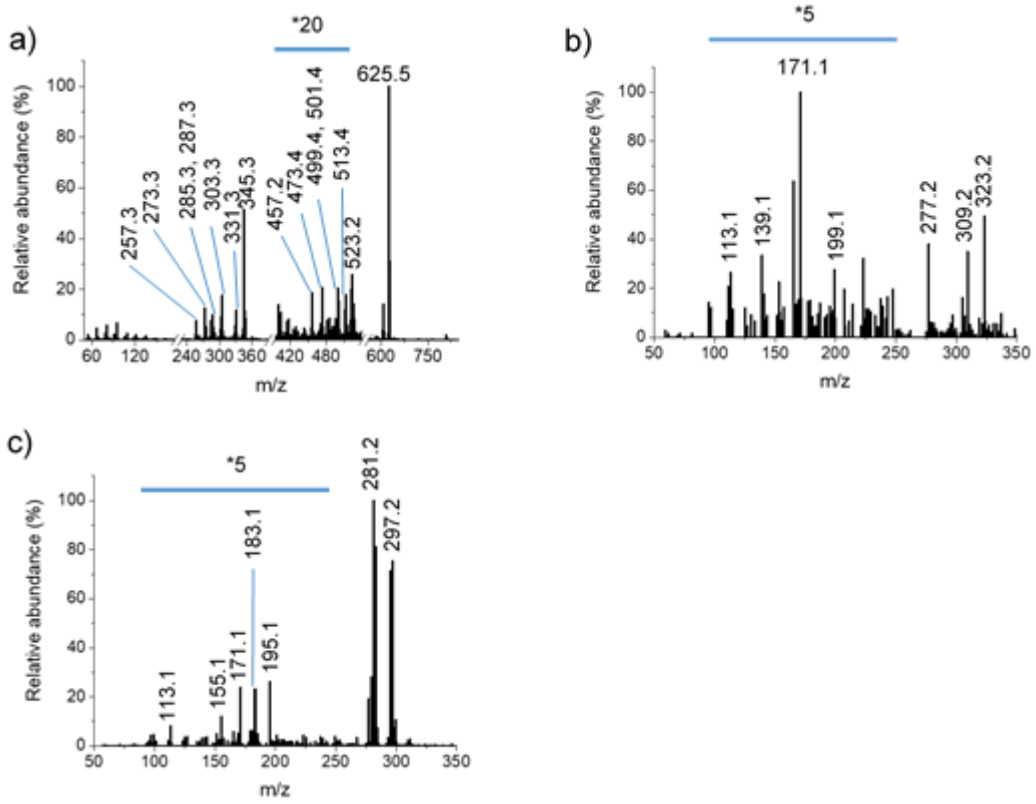

Figure S17. TENG TAP IM-MS analysis of multiple PC (36:2) isomers in an egg PC extract. a) Positive ion mode TAP product ion spectrum of the dioxolane ATD region at 6.84 ms. The $[MO+Li]^+$ ion at *m/z* 808.6 was selected as the precursor ion, which included the PC (16:0/20:2(11, 14)), PC (18:1(9)/18:1(9)), PC(18:0/18:2(9, 12)) isobars. Fragment annotations are given in Table S1b. b) Negative ion mode TAP product ion spectrum for the 20:2 $[FA+O-H]^-$ ion (*m/z*323.2) with an ATD maximum at 3.31 ms. The PC(16:0_20:2(11,14)) $[MO+OAc]^-$ ions at *m/z* 860.6 were selected as the precursor ions. c) Negative ion mode TAP product ion spectrum for the 18:1 $[FA+O-H]^-$ ion (*m/z* 297.2) with an ATD maximum at 3.09 ms. The PC(18:1(9)_18:1(9)) $[MO+OAc]^-$ ion, also at *m/z* 860.6, was selected as the precursor ion.

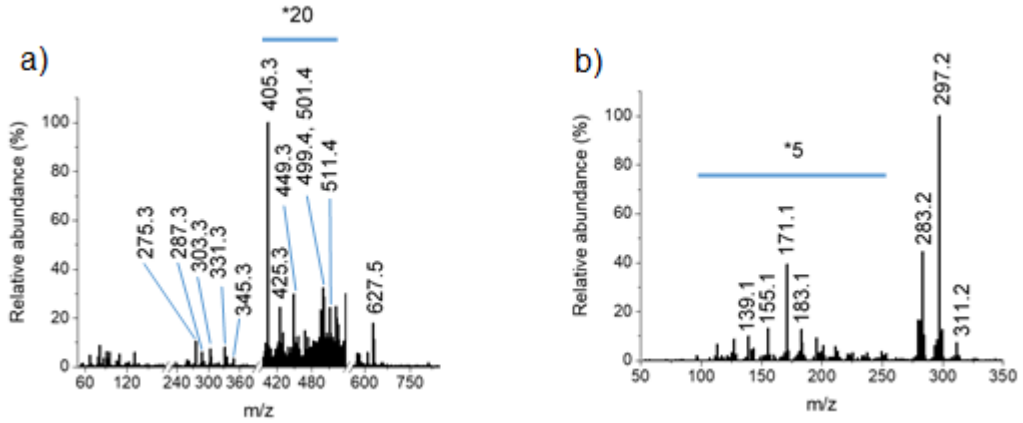

Figure S18. TENG TAP IM-MS analysis of multiple PC (36:1) isomers in an egg PC extract. a) Positive ion mode TAP product ion spectrum of the dioxolane ATD region at 6.84 ms. The $[MO+Li]^+$ ion at *m/z* 810.6 was selected as the precursor ion, which included the PC(16:0/20:1(11)), PC(18:0/18:1(9)), PC (18:1(9)/18:0) isobars. Fragment annotations are given in Table S1b. b) Negative ion mode TAP product ion spectrum for the 18:1 $[FA+O-H]^-$ ion (*m/z* 297.2) with an ATD maximum at 3.09 ms. The $[MO+OAc]^-$ ion at *m/z* 862.6 for PC(16:0_20:1(11)), and PC(18:0_18:1(9)) was selected as the precursor ion.

Table S1. Ions detected in positive ion mode during the TENG TAP IM-MS analysis of a chicken egg extract. The table describes the precursor ions detected along with the different fragment ions enabling C=C bond location pinpointing and chain *sn*-position assignment. a) $[M+Li]^+$, and b) $[MO+Li]^+$.

a)

Detected PCs		Precursor ion *m/z* $[M+Li]^+$	Fragment *m/z* $Route_{11}$ (R11, R12)	Fragment *m/z* $Route_{21}$ (R21)
PC(34:2)	16:1/18:1	764.6	301.3, 287.3	345.3
	18:2/16:0		327.3, 261.1	319.3
	16:0/18:2		303.3, 285.3	343.3
PC(34:1)	16:0/18:1	766.6	303.3, 287.3	345.3
	18:1/16:0		329.3, 261.3	319.3
PC(36:4)	16:0/20:4	788.6	303.3, 309.3	367.3
	20:4/16:0		351.3, 261.3	319.3
	18:2/18:2		327.3, 285.3	343.3
PC(36:3)	16:0/20:3	790.6	303.3, 311.3	369.3
	20:3/16:0		353.3, 261.2	319.3
	18:1/18:2		329.3, 285.2	343.3
	18:2/18:1		327.3, 287.3	345.3
PC(36:2)	16:0/20:2	792.6	303.3, 313.3	371.3
	18:1/18:1		329.3, 287.3	345.3
	18:0/18:2		331.3, 285.3	343.3
PC(36:1)	16:0/20:1	794.6	303.3, 315.3	373.3
	18:0/18:1		331.3, 287.3	345.3
	18:1/18:0		329.3, 289.3	347.3
PC(38:6)	16:0/22:6	812.6	303.3, 333.3	391.3
	22:6/16:0		375.3. 261.3	319.3
	18:1/20:5		329.3, 307.3	365.3
PC(38:5)	16:0/22:5	814.6	303.3, 335.3	393.3
	22:5/16:0		377.3, 261.3	319.3
	18:1/20:4		329.3, 309.3	367.3
PC(38:4)	16:0/22:4	816.6	303.3, 337.3	395.3
	18:0/20:4		331.3, 309.3	367.3
	20:4/18:0		351.3, 289.3	347.3

b)

Detected PCs		$[MO+Li]^+$ Precursor ion *m/z*	Double bond diagnostic fragment *m/z*	Fragment *m/z* $Route_{11}$ ($Sn1_{11}$, $Sn1_{12}$)	Fragment *m/z* $Route_{21}$ ($Sn2_{21}$)
PC(34:2)	16:1/18:1	780.6	18:1 (9) 471.4, 455.4 16:1 (9) 499.4, 483.4	317.3 (301.3+O), 303.3 (287.3+O)	361.3 (345.3+O)
	18:2/16:0		18:2 (9) 473.4, 457.4 (12) 513.4, 497.4	343.3 (327.3+O), 261.3	319.3
	16:0/18:2			303.3, 301.3 (285.3+O)	359.3 (343.3+O)
PC(34:1)	16:0/18:1	782.6	18:1 (9) 473.4, 457.4	303.3, 303.3 (287.3+O)	361.3 (345.3+O)
	18:1/16:0			345.3 (329.3+O), 261.3	335.3 (319.3+O)
PC(36:4)	16:0/20:4	804.6	20:4 (5) 401.3, 417.3, (8) ND[1], 455.4	303.3, 325.3 (309.3+O)	383.3 (367.3+O)

	20:4/16:0		(11) 479.4, 495.4 (14) 519.4, 535.4	367.3 (351.3+O), 261.3	319.3
	18:2_18:2		18:2 (9) 497.4, 481.4 (12) 537.4, 521.4	343.3 (327.3+O), 301.3 (285.3+O)	359.3 (343.3+O)
PC(36:3)	16:0/20:3	806.6	20:3 (5) 401.3, 417.3 (8) 455.4, ND (11) 495.4, ND	303.3, 327.3 (311.3+O)	ND
	20:3/16:0			369.3 (353.3+O), ND	319.3
	18:1/18:2		18:2 (9) 499.4, 483.4 (12) 539.4, 523.4, 18:1 (9) 497.4, 481.4	345.3 (329.3+O), 301.3 (285.3+O)	359.3 (343.3+O)
	18:2/18:1			343.3 (327.3+O), 303.3 (287.3+O)	ND
PC(36:2)	16:0/20:2	808.6	20:2 (11) 501.4, 485.4, (14) 541.5, 525.4	303.3, 329.3 (313.3+O)	387.3 (371.3+O)
	18:1/18:1		18:1(9) 499.4, 483.4.	345.3 (329.3+O), 303.3 (287.3+O)	361.3 (345.3+O)
	18:0/18:2		18:2(9) 501.4, 485.4, (12) 529.4, 513.4	331.3, 301.3 (285.3+O)	359.3 (343.3+O)
PC(36:1)	16:0/20:1	810.6	20:1 ND, ND	303.3, 331.3 (315.3+O)	ND
	18:0/18:1		18:1 (9) 501.4, 485.4	331.3, 303.3 (287.3+O)	361.3 (345.3+O)
	18:1/18:0			345.3 (329.3+O), 289.3	347.3

[1]ND: not detected

Table S2. Ions detected in negative ion mode during TENG TAP IM-MS analysis of a chicken egg extract. The table describes the precursor ions detected along with the different fragment ions enabling C=C bond location pinpointing and/or chain *sn*-position assignment. a) $[M+OAc]^-$, and b) $[MO+OAc]^-$.

a)

Detected PC		$[M+OAc]^-$ precursor ion *m/z*	Fatty acyl chains composition fragments	*sn* composition fragments
PC(34:2)	16:1_18:1	816.6	253.2 (16:1), 281.2 (18:1)	ND, ND,_ 478.3,460.3
	16:0_18:2		255.2 (16:0), 279.2 (18:2)	504.3, 486.3, 480.3, 462.3
PC(34:1)	16:0_18:1	818.6	255.2 (16:0), 281.2 (18:1)	506.3, 488.3, 480.3, 462.3
PC(36:4)	16:0_20:4	840.6	255.2 (16:0), 303.2 (20:4)	528.3, 510.3, 480.3, 462.3
	18:2_18:2		279.2 (18:2)	504.3, 486.3
PC(36:3)	16:0_20:3	842.6	255.2 (16:0), 305.2 (20:3)	ND, 512.3, 480.3,462.3
	18:1_18:2		281.2 (18:1), 279.2 (18:2)	506.3, 504.3, 488.3, 486.3
PC(36:2)	16:0_20:2	844.6	255.2 (16:0), 307.2 (20:2)	ND, ND, 480.3, 462.3
	18:1_18:1		281.2 (18:1)	506.3,488.3
	18:0_18:2		283.2 (18:0), 279.2 (18:2)	508.3, 504.3, 490.3, 486.3
PC(36:1)	16:0_20:1	846.6	255.2 (16:0), 309.2 (20:1)	ND, ND, 480.3, 462.3
	18:0_18:1		283.2 (18:0), 281.2 (18:1)	508.3, 506.3, 490.3, 488.3
PC(38:6)	16:0_22:6	864.6	255.2 (16:0), 327.2 (22:6)	552.3, 534.3, 480.3, 462.3
	18:1_20:5		281.3 (18:1), 301.2 (20:5)	ND, 508.3, 506.3, ND
PC(38:5)	16:0_22:5	866.6	255.2 (16:0), 329.2 (22:5)	536.3, 554.3, 480.3, 462.3
	18:1_20:4		281.2 (18:1), 303.3 (20:4)	ND, 510.3, 506.3, 488.3
PC(38:4)	16:0_22:4	868.6	255.2 (16:0), 331.3 (22:4)	538.3, ND, 480.3, 462.3
	18:0_20:4		283.2 (18:0), 303.2 (20:4)	528.3, 510.3, 508.3, 490.3

b)

Detected PC		$[MO+OAc]^-$ precursor ion *m/z*	Double bond diagnostic fragments	*sn* composition fragments
PC(34:2)	16:1_18:1	832.6	(9) 171.1, 155.1	522.3 (506.3+O), 504.3 (488.3+O), 494.3 (478.3+O), 476.3 (460.3+O)
	16:0_18:2		(9) 171.1, 155.1. (12) 211.1, 195.1	520.3 (504.3+O), 502.3 (486.3+O), 480.3, 462.3

PC(34:1)	16:0_18:1	834.6	(9) 171.1, 155.1. (11) 199.1, 183.1	522.3 (506.3+O), 504.3 (488.3+O), 480.3, 462.3
PC(36:4)	16:0_20:4	856.6	(5) 99.1, ND (8) 139.1, 155.1 (11) ND, 195.1 (14) 219.1, 235.1	544.3 (528.3+O), ND (510.3+O), 480.3, 462.3
	18:2_18:2		(9) 171.1, 155.1, (12) ND, 195.1	520.3 (504.3+O) 502.3 (486.3+O)
PC(36:3)	16:0_20:3	858.6	(8) 141.1, 157.1 (11) 181.1, 197.1 (14) 219.2, 235.2	ND, ND,_480.3, 462.3
	18:1_18:2		(9) 171.1, 155.1 (12) ND, 195.1	522.3 (506.3+O), 520.3 (504.3+O), 504.3 (488.3+O), ND
PC(36:2)	16:0_20:2	860.6	(11) 183.1, 199.1 (14) 223.2, 239.2	ND, ND, 480.3, ND
	18:1_18:1		(9) 171.1, 155.1	522.3 (506.3+O), 504.3 (488.3+O)
	18:0_18:2		(9) 171.1, 155.1 (12) 195.1, ND	508.3, 520.3 (504.3+O), 490.3, 502.3 (486.3+O)
PC(36:1)	16:0_20:1	862.6	(11) 199.1, 183.1 (3.6 ms)	ND, ND, 480.3, 462.3
	18:0_18:1		(9) 171.1, 155.1 (3.09 ms)	508.3, 522.3 (506.3+O), 490.3, 504.3 (488.3+O)

[1]ND: not detected

References

(1) Bouza, M.; Li, Y.; Wu, C.; Guo, H.; Wang, Z. L.; Fernández, F. M. Large-Area Triboelectric Nanogenerator Mass Spectrometry: Expanded Coverage, Double-Bond Pinpointing, and Supercharging, *Journal of the American Society for Mass Spectrometry* **2020**, *31*, 727-734.
(2) Lakhian, V.; Dickson-Anderson, S. E. Aqueous phase corona discharge for the reduction of nitrate in solution, *Environmental Science: Water Research & Technology* **2018**, *4*, 795-805.
(3) Giardina, A.; Schiorlin, M.; Marotta, E.; Paradisi, C. Atmospheric Pressure Non-thermal Plasma for Air Purification: Ions and Ionic Reactions Induced by dc+ Corona Discharges in Air Contaminated with Acetone and Methanol, *Plasma Chemistry and Plasma Processing* **2020**, *40*, 1091-1107.
(4) Hsu, F.-F.; Turk, J.; Thukkani, A. K.; Messner, M. C.; Wildsmith, K. R.; Ford, D. A. Characterization of alkylacyl, alk-1-enylacyl and lyso subclasses of glycerophosphocholine by tandem quadrupole mass spectrometry with electrospray ionization, *Journal of Mass Spectrometry* **2003**, *38*, 752-763.
(5) Williams, P. E.; Klein, D. R.; Greer, S. M.; Brodbelt, J. S. Pinpointing Double Bond and sn-Positions in Glycerophospholipids via Hybrid 193 nm Ultraviolet Photodissociation (UVPD) Mass Spectrometry, *Journal of the American Chemical Society* **2017**, *139*, 15681-15690.
(6) Kozlowski, R. L.; Mitchell, T. W.; Blanksby, S. J. A rapid ambient ionization-mass spectrometry approach to monitoring the relative abundance of isomeric glycerophospholipids, *Scientific Reports* **2015**, *5*, 9243.